JEM Journal of Experimental Medicine

ARTICLE

PIK3IP1/TrIP restricts activation of T cells through inhibition of PI3K/Akt

Uzodinma U. Uche[1,2], Ann R. Piccirillo[1], Shunsuke Kataoka[3], Stephanie J. Grebinoski[4], Louise M. D'Cruz[1], and Lawrence P. Kane[1]

Phosphatidylinositol-3 kinases (PI3Ks) modulate cellular growth, proliferation, and survival; dysregulation of the PI3K pathway can lead to autoimmune disease and cancer. PIK3IP1 (or transmembrane inhibitor of PI3K [TrIP]) is a putative transmembrane regulator of PI3K. TrIP contains an extracellular kringle domain and an intracellular domain with homology to the inter-SH2 domain of the PI3K regulatory subunit p85, but the mechanism of TrIP function is poorly understood. We show that both the kringle and p85-like domains are necessary for TrIP inhibition of PI3K and that TrIP is down-modulated from the surface of T cells during T cell activation. In addition, we present evidence that the kringle domain may modulate TrIP function by mediating oligomerization. Using an inducible knockout mouse model, we show that TrIP-deficient T cells exhibit more robust activation and can mediate clearance of *Listeria monocytogenes* infection faster than WT mice. Thus, TrIP is a negative regulator of T cell activation and may represent a novel target for immune modulation.

Introduction

Phosphatidylinositide-3-kinases (PI3Ks) are a family of lipid kinases that play important intracellular signaling roles in cellular processes such as proliferation, motility, growth, intracellular trafficking, differentiation, and survival (Cantley, 2002; Fruman, 2007; Han et al., 2012). There are three main classes of PI3K. Class I PI3Ks, which are prevalent in immune cells, are composed of two subunits: a regulatory subunit (p85) and a catalytic subunit (p110; Fruman et al., 1998; Fresno Vara et al., 2004; Engelman, 2009). During T cell receptor activation, PI3K is recruited to the plasma membrane via the SH2 domain of the p85 subunit. The associated p110 subunit is then activated to phosphorylate phosphatidylinositol 4,5-bisphosphate (PIP_2) and produces phosphatidylinositol (3,4,5)-trisphosphate (PIP_3). PIP_3 interacts with the pleckstrin homology domain of Akt, causing a conformational change that allows PDK1 (kinase 3-phosphoinositide–dependent protein kinase-1) to partially activate Akt by phosphorylating threonine 308 (T308). Full activation of Akt is achieved by mTORC2-mediated phosphorylation at serine 473 (S473) and facilitates such processes as cell growth, cell cycle progression, and cell survival. It is therefore not surprising that Akt amplification due to dysregulation of PI3K has been implicated in many cancers. This has prompted the development of PI3K pathway inhibitors as a potential cancer treatment modality (Engelman, 2009).

Several negative regulators of PI3K have been identified (Carracedo and Pandolfi, 2008; Antignano et al., 2010; Agoulnik et al., 2011; Dillon and Miller, 2014). Thus, PTEN (phosphatase and tensin homologue deleted on chromosome 10) and SHIP-1 (SH2-containing inositol 5′-phosphatase) are phosphatases that dephosphorylate PIP_3 to PIP_2, thereby inhibiting downstream signaling in the PI3K pathway. INPP4B (inositol polyphosphate 4-phosphatase type II) has been shown to dephosphorylate PIP_2, thereby playing a role in the negative regulation of the PI3K pathway. Several studies have shown that loss-of-function mutations or deletions of these phosphatases can lead to dysregulated PI3K activity.

Although the above phosphatases act downstream of PI3K, PIK3IP1 (PI3K-interacting protein-1, which we will refer to as TrIP [transmembrane inhibitor of PI3K] for simplicity) is a recently identified inhibitor that acts upstream of the aforementioned phosphatases (Zhu et al., 2007; DeFrances et al., 2012). TrIP is a transmembrane protein composed of two main domains, an extracellular kringle domain and an intracellular tail that includes a motif similar to the p110-binding inter-SH2 domain found in the p85 subunit of PI3K. Overexpression of TrIP in mouse hepatocytes leads to a reduction in PI3K signaling and suppression of hepatocyte carcinoma development (He et al., 2008). Furthermore, recent work in cancer genetics highlights the transcriptional down-regulation of TrIP as a contributing factor to dysregulated PI3K signaling in tumorigenesis (Wong et al., 2014). Although it has been shown that TrIP inhibits PI3K by binding

[1]Department of Immunology, University of Pittsburgh School of Medicine, Pittsburgh, PA; [2]Interdisciplinary Biomedical Graduate Program, University of Pittsburgh School of Medicine, Pittsburgh, PA; [3]Asahi Kasei Pharma Corporation, Tokyo, Japan; [4]Graduate Program in Microbiology and Immunology, University of Pittsburgh School of Medicine, Pittsburgh, PA.

Correspondence to Lawrence P. Kane: lkane@pitt.edu.

the p110 subunit via the p85-like domain, the role of the kringle domain remains to be determined. Given the ability of kringle domains in other proteins to bind to various ligands, it is possible that the TrIP kringle domain may bind one or more ligands for modulation of TrIP activity (Patthy et al., 1984; Mikels et al., 2009; Christen et al., 2010). Because TrIP is highly expressed in immune cells, particularly mast cells and T cells (DeFrances et al., 2012), we wanted to investigate how the structure of TrIP enables regulation of PI3K in the context of an activated T cell.

In this study, we investigated the importance of both the kringle and p85-like domains to TrIP function in activated T cells. We also examined how cell fate decisions and immune response are regulated by TrIP. Here we show that both the extracellular kringle domain and the intracellular p85-like domain are necessary for inhibition of PI3K by TrIP. Intriguingly, we also show that cell-surface levels of TrIP are decreased upon T cell activation, which correlates with the up-regulation of PI3K pathway signaling. Using a T cell conditional knockout mouse model, we show that the loss of TrIP in T cells leads to an increase in T cell activation, which translates to stronger T helper type 1 (Th1) inflammatory potential and more rapid clearance of *Listeria monocytogenes* infection.

Results

TrIP inhibits PI3K/Akt/mTOR pathway signaling

We have previously shown that ectopic expression of TrIP in T cells can inhibit the phosphorylation of Akt and thus its activation (DeFrances et al., 2012). A more sensitive readout of PI3K/Akt/mTOR activity is analysis of ribosomal protein S6 phosphorylation (pS6) by flow cytometry (Fig. S1). To study the structural requirements of TrIP for modulation of T cell function, we evaluated pS6 in D10 T cells, a cell line with apparently normal PI3K signaling (Kane et al., 2004), in the context of ectopically expressed WT or mutant TrIP. The domain structure of TrIP is illustrated in Fig. 1 A. In the absence of a suitable antibody for detecting TrIP by flow cytometry, we transfected D10 T cells with control plasmid or Flag-tagged TrIP (WT TrIP) and monitored TrIP expression using α-Flag antibody (Fig. 1 B). 1 d after transfection, cells were stimulated with α-CD3/CD28 and analyzed by gating on GFP-expressing cells at various time points (Fig. 1, C and D). At all time points evaluated, cells with ectopic TrIP expression displayed lower pS6, compared with empty vector–transfected cells. We also noted that, in the absence of stimulation, ectopic expression of TrIP resulted in lower basal pS6. In these experiments, and those shown below, we have focused on the percentage of $pS6^+$ cells, as this event appears to mainly manifest as a digital response. As an additional readout for PI3K/Akt activity, we also measured the effect of ectopic TrIP on nuclear exclusion of FoxO1, which occurs after Akt-mediated phosphorylation (Hedrick et al., 2012). Thus, as shown by imaging flow cytometry, while CD3/CD28 stimulation resulted in rapid nuclear exit (and apparent degradation) of FoxO1, this effect was dramatically impaired in D10 cells expressing ectopic TrIP (Fig. S1, C and D). These results are consistent with previous data suggesting that TrIP inhibits PI3K activation in fibroblasts and with our earlier finding that TrIP inhibits Akt activation in T cells (Zhu et al., 2007; DeFrances et al., 2012).

The kringle and cytoplasmic domains are required for TrIP activity

The importance of the kringle domain as a ligand-binding domain in other proteins (Patthy et al., 1984; Menhart et al., 1995; Mikels et al., 2009), and the degree of homology between the p85-like domain and the inter-SH2 domain of the p85 regulatory subunit of PI3K, suggests that these two domains may play important roles in the inhibition of PI3K by TrIP. To address this, we designed Flag-tagged TrIP variants lacking either the extracellular kringle domain (Δkringle-TrIP), the entire cytoplasmic region (Δcyto-TrIP), or only the p85-like domain (Δp85-like-TrIP). These constructs were transfected, along with a GFP transfection control, into D10 T cells (Fig. 1 E) which were then stimulated with α-CD3/CD28 and analyzed by flow cytometry (after gating on GFP-positive cells; Fig. S2 A) for S6 phosphorylation (Fig. 1, F and G). While WT TrIP led to the attenuation of pS6, deletion of either the p85-like domain alone or the entire cytoplasmic region abolished the ability of TrIP to suppress pS6. Interestingly, expression of the kringle domain–deleted construct (which still possesses the p85-like domain) did not attenuate pS6. These results suggest that both the kringle and p85-like domains are essential for optimal TrIP inhibitory function.

Cell-surface TrIP is down-regulated upon T cell activation

Our data strongly support an inhibitory role for TrIP in T cells. Certain other negative regulators of T cell signaling (e.g., PTEN) are actively down-regulated to promote T cell activation (Newton and Turka, 2012; Hawse et al., 2015), so we examined how TCR activation might affect expression of TrIP protein. To replicate T cell stimulation in the presence of an APC, we used the mouse B cell lymphoma line CH27 (Haughton et al., 1986) to stimulate D10 cells. CH27 cells were either pulsed with cognate antigen (chicken conalbumin) or left unpulsed, and then mixed with D10 T cells transfected with Flag-tagged PI3KIP1. There was a notable decrease over time in Flag-TrIP expression on the surface of D10 cells (Fig. 2, A and B). Interestingly, this decreased expression corresponded with an increase of pS6 expression (Fig. 2, C and D). As observed when D10 T cells were stimulated with α-CD3/CD28 (Fig. 1), antigen-pulsed CH27 cells induced a more immediate and robust pS6 signal in T cells transfected with empty vector, compared with those transfected with WT TrIP (Fig. S2 B). These results support the model that T cells acutely modulate the expression of TrIP to promote the activation of TCR-induced PI3K signaling.

Structure–function analysis of TrIP cell-surface expression and inhibitory activity

To probe the relevance of the kringle domain for TrIP expression and function, we used the CH27/D10 system with D10 cells expressing either Flag-tagged WT or Δkringle-TrIP T cells and monitored Flag-TrIP expression and S6 phosphorylation. Since Δkringle-TrIP transfected cells showed a recovery in TCR-dependent pS6 (Fig. 1, F and G), we suspected that the absence of the kringle domain would lead to maintenance (and not down-regulation) of TrIP. As shown above, D10 cells transfected with WT TrIP and stimulated with CH27 B cells alone (without antigen) did not show significant loss of TrIP expression over time. How-

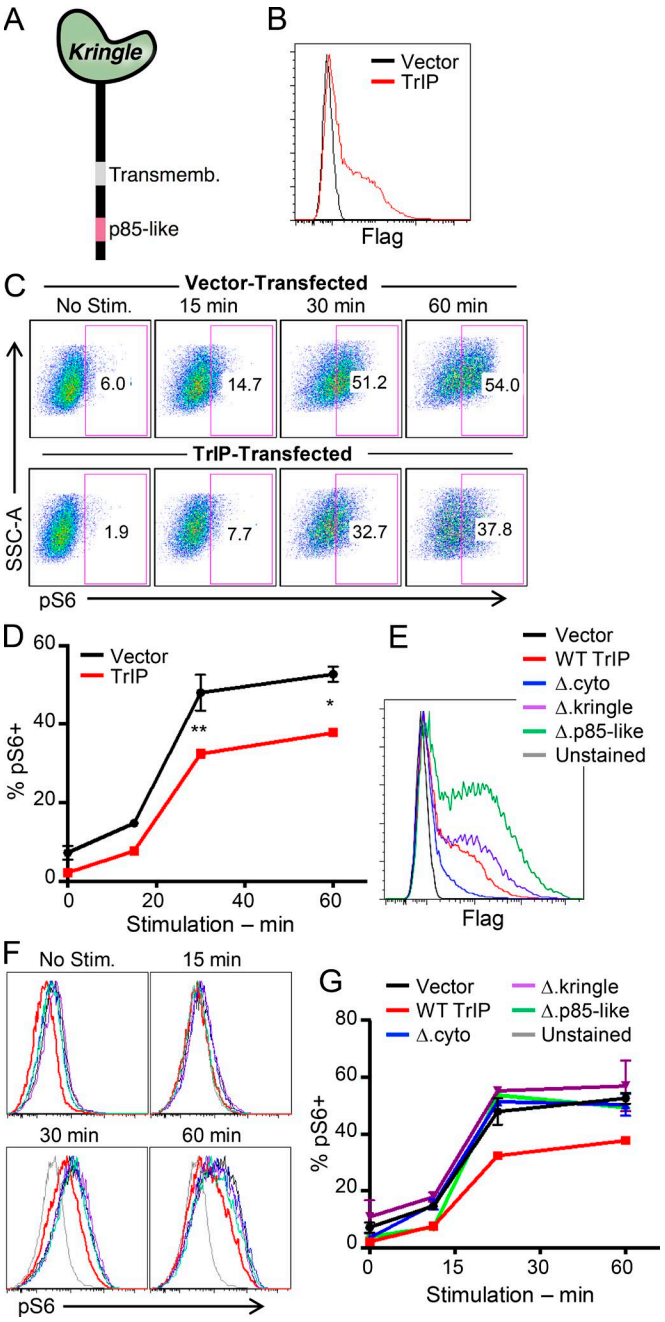

Figure 1. **The kringle and cytoplasmic domains are required for TrIP activity. (A)** Domain structure of TrIP, indicating the kringle, transmembrane, and p85-like domains. **(B)** Expression of Flag-tagged WT TrIP on transiently transfected D10 T cells. **(C)** Flow cytometric analysis of pS6 activation in control (vector) or WT TrIP-transfected D10 T cells, stimulated with anti-CD3/CD28 for the indicated times. **(D)** Quantitation of pS6 activation as shown in C. **(E)** Expression of WT and mutant Flag-tagged TrIP constructs on transfected D10 cells. **(F)** Representative histogram of pS6 staining in D10 cells transiently transfected with Flag-tagged TrIP constructs and activated with anti-CD3/CD28. **(G)** Quantitation of pS6 activation obtained from flow cytometric analysis of activated D10 cells transfected with Flag-tagged TrIP constructs, as shown in F. Cells were cotransfected with TrIP constructs along with a GFP plasmid, and GFP-positive cells were analyzed by flow cytometry for Flag and pS6 expression. Data in each panel are representative of at least three experiments. Data shown represent the mean ± SEM. P values (for TrIP versus vector) were calculated using two-way ANOVA with Sidak's multiple comparisons test. P values are represented with the following symbols: *, P = 0.01–0.05; **, P = 0.001–0.01; and ***, P < 0.001.

ever, when mixed with antigen-pulsed CH27 cells, WT TrIP-expressing D10 T cells showed a significant loss of TrIP expression (Fig. 3 A, top row, and B). In contrast, D10 cells transfected with the Δkringle-TrIP mutant did not lose surface TrIP expression when stimulated with CH27 cells (with or without antigen; Fig. 3 A, bottom row, and B). Consistent with the results above, upon mixing with antigen-pulsed CH27 cells, Δkringle-TrIP–expressing D10 T cells actually showed a more rapid increase in pS6 than cells transfected with WT TrIP (Fig. 3, C and D). These results further confirm that the kringle domain is important for the inhibitory function of TrIP and suggest the possibility that TrIP is regulated by interaction with a ligand.

In the absence of a known ligand, we designed an hCD8-TrIP chimera to investigate possible effects of ligand engagement on TrIP function. The extracellular and transmembrane regions of human CD8 were fused with the cytoplasmic tail of TrIP, expressed in D10 T cells and detected at the cell surface with hCD8 antibody (Fig. 4 A). Using a luciferase reporter driven by the NFAT promoter, we observed that expression of hCD8-TrIP on D10 T cells was not sufficient to inhibit TCR signaling (Fig. 4 B). Similarly, expression of the chimera itself did not inhibit anti-CD3/CD28–induced pS6 (Fig. 4, C and D; and Fig. S2 C). However, upon cross-linking of hCD8-TrIP with varying concentrations of anti-hCD8, we observed a decrease in anti-CD3/CD28–induced pS6 (Fig. 4, C and D; and Fig. S2 C). This was in contrast to the effects of a previously described CD8-ζ chimeric construct (Irving and Weiss, 1991), which, upon cross-linking with anti-hCD8, modestly enhanced the pS6 signal (Fig. 4, C and D). These results suggest that the kringle domain of TrIP could regulate oligomerization of the protein, either after interaction with a distinct ligand or through homo-oligomerization. To investigate the latter possibility, we coexpressed Myc-tagged WT-TrIP with Flag-tagged WT-TrIP in 293T cells and used anti-Flag beads to immunoprecipitate Flag-tagged TrIP (Fig. 4 E). Upon blotting with anti-Myc, we found that Flag-tagged WT-TrIP was able to coimmunoprecipitate Myc-tagged WT-TrIP (Fig. 4 E). This suggests that TrIP oligomerizes upon expression, which promotes its ability to inhibit PI3K signaling (as evidenced by our results from Fig. 4). However, this finding does not rule out the possibility of a trans-interacting ligand for TrIP on the APCs.

To further probe the function of the kringle domain, we next returned to the apparent down-regulation of TrIP from the surface of activated T cells. One possible mechanism that we considered for this is metalloprotease-mediated cleavage of the ecto domain (including the kringle) of TrIP, based on past work on T cell regulators like LAG-3 and Tim-3 (Li et al., 2004, 2007; Clayton et al., 2015). We transfected D10 T cells with Flag-tagged WT TrIP, then stimulated these cells with anti-CD3/CD28 mAbs, with or without an inhibitor of ADAM family metalloproteases 10 and 17, which were previously shown to mediate cleavage of LAG-3 and Tim-3. A constitutively expressed GFP construct was cotransfected to further track the transfected cells. As shown in the representative flow cytometry data in Fig. 4 F, stimulation of control vehicle-treated cells led to loss of cell-surface Flag staining, whereas the cells treated with an inhibitor of ADAM10/17 maintained Flag expression after stimulation. These results are quantified in Fig. 4 G. Thus, one mechanism for down-reg-

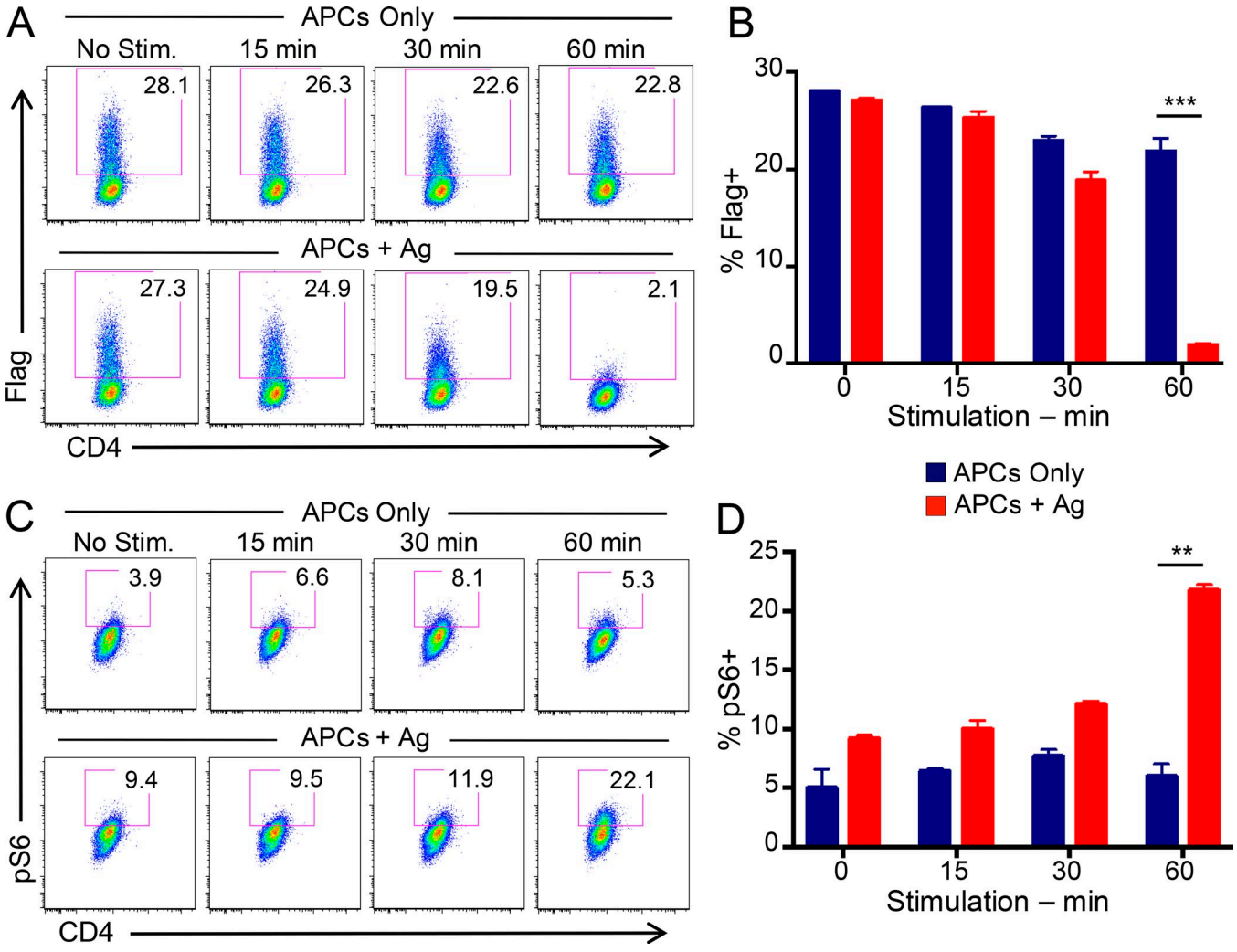

Figure 2. **Cell-surface TrIP is down-regulated during T cell activation.** D10 cells transfected with WT TrIP were mixed with CH27 B cells as APCs (± conalbumin antigen) for the given time points. **(A)** Representative flow cytometry analyzing cell-surface expression of Flag-tagged WT TrIP on D10 cells stimulated with CH27 B cells alone (top row) or plus antigen (bottom row). **(B)** Quantitation of data shown in A. **(C)** Representative flow cytometry analyzing pS6 staining in D10 cells transfected with Flag-tagged WT TrIP and stimulated with CH27 B cells alone (top row) or plus antigen (bottom row). **(D)** Quantitation of data shown in C. Data are representative of three experiments. Data shown represent the mean ± SEM. P values (compared with time 0) were calculated using two-way ANOVA with Sidak's multiple comparisons test. P values are represented with the following symbols: *, P = 0.01–0.05; **, P = 0.001–0.01; and ***, P < 0.001.

ulation of TrIP after T cell activation appears to be through ADAM10/17-mediated shedding of the kringle domain.

To determine whether inducible down-regulation of TrIP only occurs in the context of stimulation by antigen and APCs (which may express a ligand for TrIP), we stimulated transfected D10 cells with α-CD3/CD28 and evaluated the surface expression of TrIP at various time points in the absence of APC and cognate antigen using the α-Flag antibody. Thus, we observed that even after CD3/CD28 stimulation, without APCs, WT TrIP expression was still down-regulated (Fig. 5, A and B) with a concomitant up-regulation of pS6 (Fig. S2 D). In contrast, neither Δcyto-TrIP (Fig. 5, A and B), Δkringle-TrIP, nor Δp85-TrIP (Fig. 5 C) expression was down-regulated by stimulation with CD3 and CD28 Abs. However, despite the fact that these TrIP mutants were not down-regulated from the cell surface, they still failed to inhibit pS6 (Fig. S2, D and E), suggesting additional levels of regulation.

The p85-like domain of TrIP interacts with p110δ PI3K

TrIP has been shown to interact with the PI3K catalytic subunits p110α/β in mouse embryonic fibroblast cells, via a p85-like domain with ∼80% homology to the inter-SH2 domain of the PI3K regulatory subunit p85 (Zhu et al., 2007). However, it is not known whether TrIP can also interact with p110δ, which is the main catalytic subunit of PI3K activated by TCR signaling (Okkenhaug and Vanhaesebroeck, 2003). To test a possible interaction of p110δ with the p85-like domain of TrIP, we transiently transfected 293 cells with Flag-tagged WT TrIP or Δp85-TrIP, along with HA-tagged p110δ, and performed coimmunoprecipitation and Western blot analysis (Fig. 5 D, top). Thus, WT TrIP could coimmunoprecipitate p110δ-PI3K; however, there was a significant reduction in the ability of Δp85-TrIP to coimmunoprecipitate p110δ (Fig. 5 D, top, last lane). These results are consistent with a previous report that examined the inter-

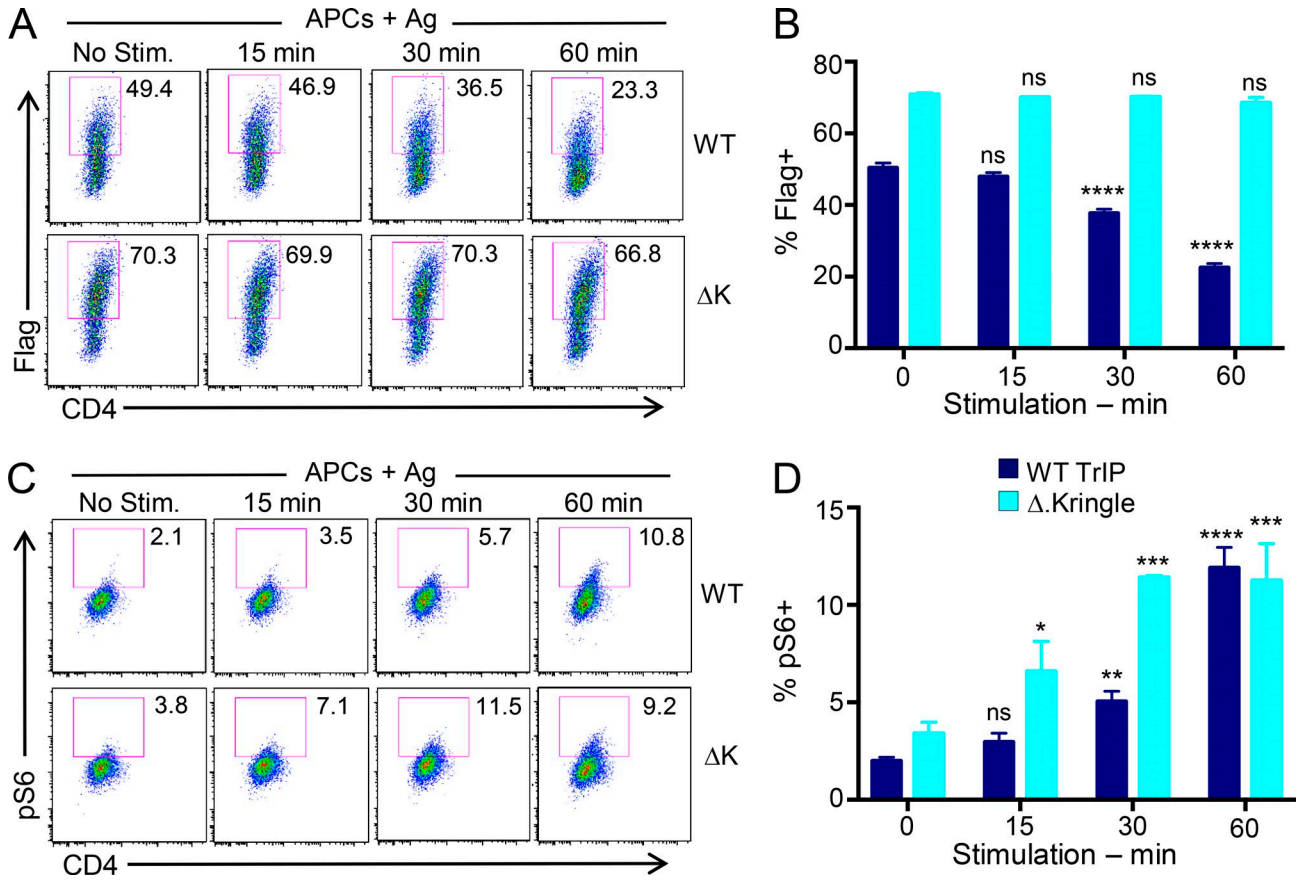

Figure 3. **The kringle domain regulates TrIP expression and function.** D10 cells transiently transfected with Flag-tagged WT or Δkringle TrIP were mixed with CH27 B cells plus antigen for the indicated times. **(A)** Representative flow cytometry analyzing cell-surface expression of Flag-tagged WT (top row) or Δkringle (bottom row) TrIP on D10 cells stimulated with CH27 B cells plus antigen. **(B)** Quantitation of data shown in A. **(C)** Representative flow cytometry analyzing pS6 staining in the same cells as in A. **(D)** Quantitation of data shown in C. Data are representative of three experiments. P values (compared with time 0) were calculated using one-way ANOVA with Dunnett's multiple comparisons test. P values are represented with the following symbols: *, P = 0.01–0.05; **, P = 0.001–0.01; ***, P = 0.0001–0.001; and ****, P < 0.0001. Data shown represent the mean ± SEM.

action of TrIP with other p110 isoforms in fibroblasts (Zhu et al., 2007) and suggest that TrIP may inhibit T cell activation through effects on p110δ.

Deletion of TrIP leads to dysregulation of T cell activation

To assess the function of TrIP in T cells in vivo, we generated mice with LoxP-flanked (floxed) *Pik3ip1* alleles (Pik3ip1$^{fl/fl}$) and bred them to mice with a CD4-driven Cre recombinase transgene. Mice with CD4-Cre alone were used as controls. In the absence of a suitable TrIP antibody, T cells from spleen and lymph nodes of naive homozygous (CD4-Cre × *Pik3ip1*$^{fl/fl}$) and heterozygous (CD4-Cre × *Pik3ip1*$^{fl/wt}$) TrIP conditional knockout mice were screened by RT-PCR for TrIP mRNA expression and compared with WT mice (CD4-Cre × *Pik3ip1*$^{wt/wt}$; Fig. S3 A). Analysis of thymus and spleen from these mice showed similar percentages of CD4 and CD8 T cells in all compartments as well as normal numbers of natural T regulatory cells (Foxp3$^+$CD25$^+$), suggesting that T cell development was largely normal (Fig. S3, B and C). Although we did not note any obvious signs of widespread basal inflammation, we assessed more directly whether deletion of TrIP might result in spontaneous activation of peripheral T cells by staining for the early activation markers CD69 and CD25. As shown in Fig. S3 D, these markers were expressed at equivalent, minimal, levels in TrIP-deficient versus WT T cells. Thus, T cell–specific deletion of TrIP does not grossly affect T cell development or homeostasis.

Based on data shown above and previously published findings (Zhu et al., 2007; DeFrances et al., 2012), we predicted that deleting TrIP in primary T cells would lead to enhanced TCR signaling, especially through the PI3K/Akt pathway. We thus stimulated lymphocytes from WT and conditionally deleted TrIP (KO) age-matched mice with α-CD3/CD28 for varying times and evaluated early T cell activation by pS6 and CD69 expression. After stimulation, TrIP KO T cells showed significantly higher pS6 at later time points (1–4 h; Fig. 6, A and B; representative histograms in Fig. S3 E). These data are consistent with our observation of more robust Akt phosphorylation at T308 and especially S473 in peripheral T cells lacking TrIP (Fig. 6, C and D). As with ectopic expression of TrIP in D10 T cells (Fig. S1, C and D), we measured the effect that deletion of TrIP would have on nuclear exclusion of FoxO1, a direct target of Akt phosphorylation. Using imaging flow cytometry, we noted that even resting, unstimulated, TrIP KO T cells displayed a significant reduction in nuclear FoxO1, compared with WT T cells (Fig. 6, E and F). Furthermore, although WT T

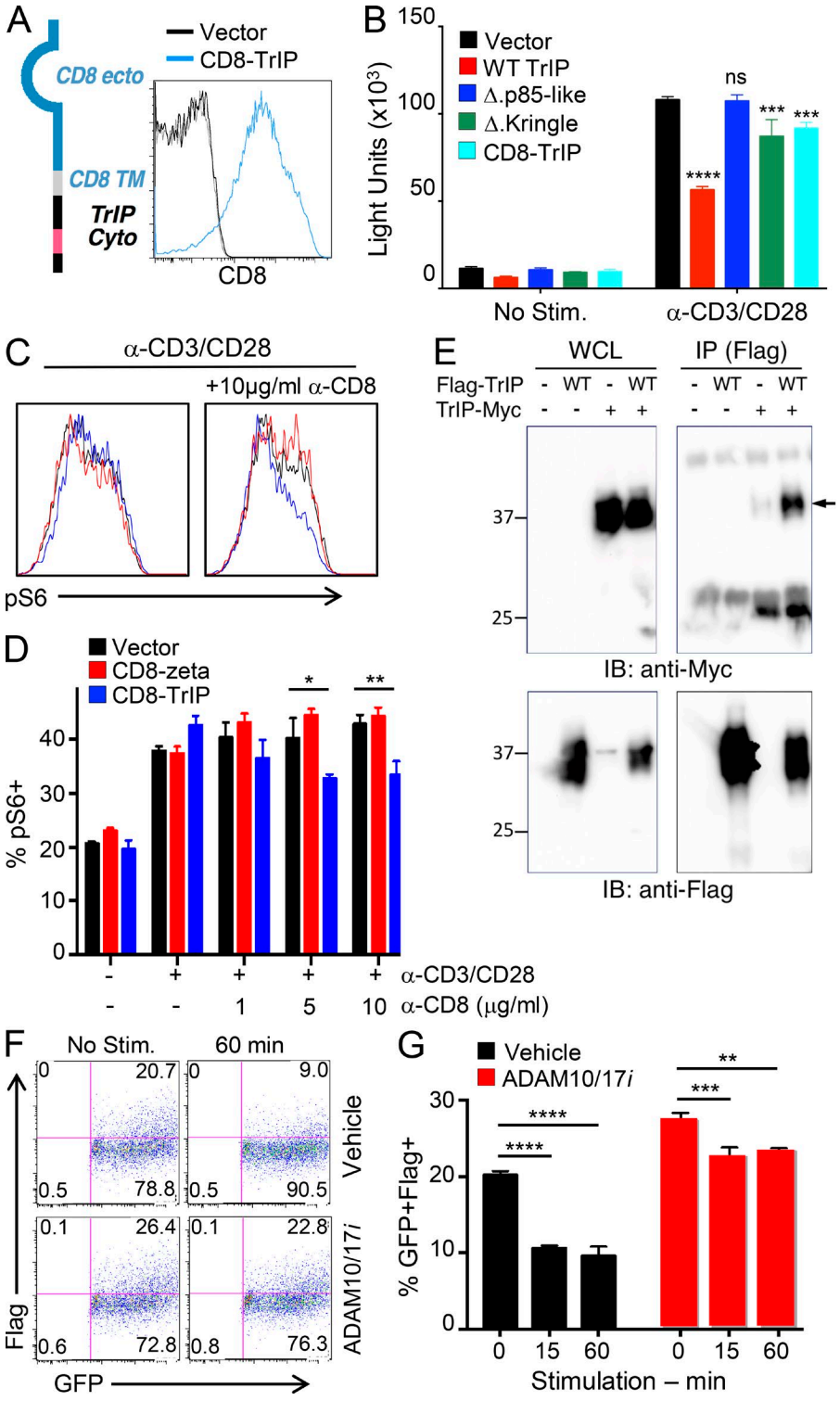

Figure 4. **Role of the ecto domain in TrIP function and regulation. (A)** Structure of ecto hCD8-mPIK3IP cytoplasmic chimera and its expression on transfected D10 cells. **(B)** D10 cells were transfected with the indicated TrIP constructs, plus an NFAT/AP1-luciferase construct, stimulated the next day with anti-CD3/CD28, followed by determination of luciferase activity. P values (compared with vector) were calculated using one-way ANOVA with Dunnett's multiple comparisons test. **(C)** Flow cytometry analysis of pS6 after stimulation of D10 cells transiently transfected with hCD8-TrIP in the presence of 10 μg/ml anti-hCD8. **(D)** Quantification of pS6 after stimulation of hCD8-TrIP transfected D10 cells in the presence of varying concentrations of anti-hCD8. P values (compared with vector) were calculated using one-way ANOVA with Dunnett's multiple comparisons test. **(E)** Detection of TrIP dimerization. 293T cells were transfected with Flag-tagged TrIP ± Myc-tagged TrIP. Whole cell lysates (WCL; left panels) or anti-Flag immunoprecipitations (IP; right panels) were blotted with anti-Myc (upper panels) or with anti-Flag mAb (lower panels). IB, immunoblot. **(F and G)** D10 T cells were transfected with Flag-TrIP plus a plasmid encoding eGFP. The next day, cells were stimulated with anti-CD3/CD28 Abs for the indicated times, with or without 1 μM GW280264X, an inhibitor of ADAM10/17. Flag staining and GFP expression were determined by flow cytometry. Representative data are shown in F, and average data of quadruplicate samples are in G. P values (compared with time 0) were calculated using two-way ANOVA with Tukey's multiple comparisons test. Data are representative of three experiments (A–E) or two experiments (F and G). P values are represented with the following symbols: *, P = 0.01–0.05; **, P = 0.001–0.01; ***, P < 0.001; and ****, P < 0.0001. Data shown represent the mean ± SEM.

cells displayed a loss of nuclear FoxO1 after anti-CD3/CD28 stimulation, TrIP KO T cells exhibited an even more rapid exclusion of FoxO1 from the nucleus, with an accompanying decrease in total FoxO1 staining, consistent with the lower stability of cytoplasmic FoxO1 (Hedrick et al., 2012). Taken together, these results demonstrate that the loss of TrIP in primary T cells promotes more efficient TCR signaling and early T cell activation, especially through the PI3K/Akt/mTOR signaling pathway.

Deletion of TrIP enhances Th1 T cell polarization and inhibits induced T regulatory cell (iTreg) generation

Previous research suggested that higher PI3K signaling may lead to enhanced Th1 potential, whereas lower levels of PI3K would favor generation of iTregs (He et al., 2008; Sauer et al., 2008). Based on our findings, we reasoned that T cell polarization toward a pro-inflammatory phenotype would be enhanced in TrIP KO T cells. We isolated naive CD4⁺ T cells from WT and KO

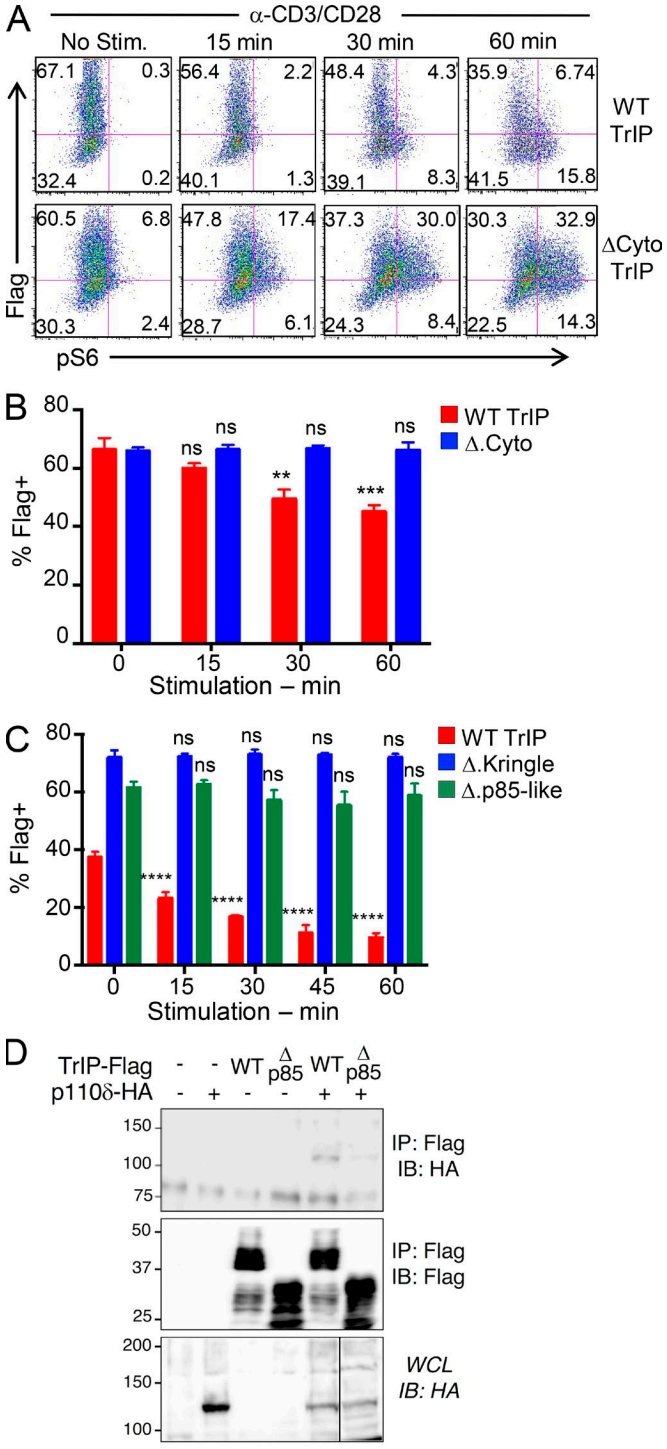

Figure 5. **Role of the cytoplasmic domain in TrIP function.** D10 cells were transfected with control, WT TrIP, or Δcyto-TrIP and stimulated with anti-CD3/CD28. **(A)** Representative flow cytometric analysis of Flag-tagged TrIP and pS6 expression of cells transfected with WT TrIP (top row) or Δcyto-TrIP (bottom row). **(B)** Quantitation of Flag expression over the course of stimulation; quantitation of total pS6⁺ cells at different time points. P values (compared with time 0) were calculated using two-way ANOVA with Holm–Sidak's multiple comparisons test. **(C)** TrIP surface expression (left) and pS6 staining (right) of cells expressing WT, Δkringle, or Δp85-like TrIP, after stimulation with anti-CD3/CD28, as in A and B. P values (compared with time 0) were calculated using one-way ANOVA with Dunnett's multiple comparisons test. **(D)** The cytoplasmic p85-like domain of TrIP binds to p110δ. 293 cells were transiently transfected with Flag-tagged WT TrIP and p85Δ-TrIP along with HA-tagged p110δ, as indicated. Top: Coimmunoprecipitation and Western blot analysis of TrIP and p110δ. Middle: Immunoprecipitation (IP) fractions showing immunoprecipitated Flag-tagged (TrIP) protein. Bottom: Whole cell lysate (WCL) showing HA-tagged (p110δ) protein expression. IB, immunoblot; HA, influenza hemagglutinin (98-106) epitope tag. Data are representative of three experiments. P values are represented with the following symbols: **, P = 0.001–0.01; ***, P = 0.0001–0.001; and ****, P < 0.0001. Data shown represent the mean ± SEM.

mice and cultured them with α-CD3/CD28 mAbs for 3 d under neutral (no polarization), Th0 (suppression of all polarization), Th1, Th17, and iTreg skewing conditions. At the end of culture, cells were restimulated with PMA/ionomycin for 4 h and then evaluated for Th1 (T-bet and IFN-γ), Th17 (RORγt and IL17a), and iTreg (CD25 and Foxp3) phenotype. Thus, we noted a significant increase in the number of cells producing IFN-γ in TrIP KO T cell cultures, compared with WT cells, especially under Th0 and Th1, and even iTreg, conditions (Fig. 7 A). Interestingly, we observed a smaller, but reproducible, decrease in the number of TrIP KO T cells making IL-17a, specifically under Th17 polarization conditions (Fig. 7 B). More strikingly, we found that TrIP-deficient T cells cultured under iTreg-generating conditions were significantly less efficient at producing Foxp3⁺CD25⁺ iTreg (Fig. 7, C and D). This result is consistent with previous findings that PI3K/Akt/mTOR signaling suppresses the generation of iTreg (Sauer et al., 2008). Interestingly, when we assessed the expression of *Pik3ip1* mRNA after culturing under various Th polarization conditions, we found that *Pik3ip1* was severely down-regulated in Th0 and Th1 cells. By contrast, *Pik3ip1* was maintained at a somewhat higher level in iTreg, although still not as high as naive cells (Fig. 7 E), consistent with an apparent requirement for weaker PI3K signaling in Treg (Huynh et al., 2014).

To determine whether the difference in Th1 polarization was actually due to enhanced PI3K activity, we performed the Th1 differentiation assay with the addition of moderate concentrations of PI3K/Akt pathway inhibitors. Specifically, we employed an Akt1/2 inhibitor (Akt*i*-1/2), a pan-PI3K inhibitor (LY294002), and a selective p110δ inhibitor (IC-87114). Cells were stimulated with α-CD3/CD28 as in Fig. 7 and cultured under Th1 conditions in the presence of varying concentrations of the PI3K inhibitors. At the end of culture, cells were restimulated with PMA/ionomycin and evaluated by flow cytometry for IFN-γ expression. We found that IFN-γ production by KO cells was significantly inhibited by all three inhibitors tested, at concentrations as low as 0.5 µM (Fig. 8, A and B). Consistent with p110δ being the most prevalent catalytic subunit of PI3K linked to TCR signaling, IC-87114 was the most potent inhibitor at all concentrations. Overall, we observed a reduction of IFN-γ production by both WT and TrIP KO T cells in the presence of inhibitors, but this inhibition was more distinct with the KO cells. These results support the idea that the high IFN-γ production by TrIP KO T cells is due to a loss of TrIP inhibition of PI3K.

Enhanced activation and in vivo function of T cells lacking TrIP

We returned to the question of how TrIP regulates early T cell activation and whether this translates to downstream effects on

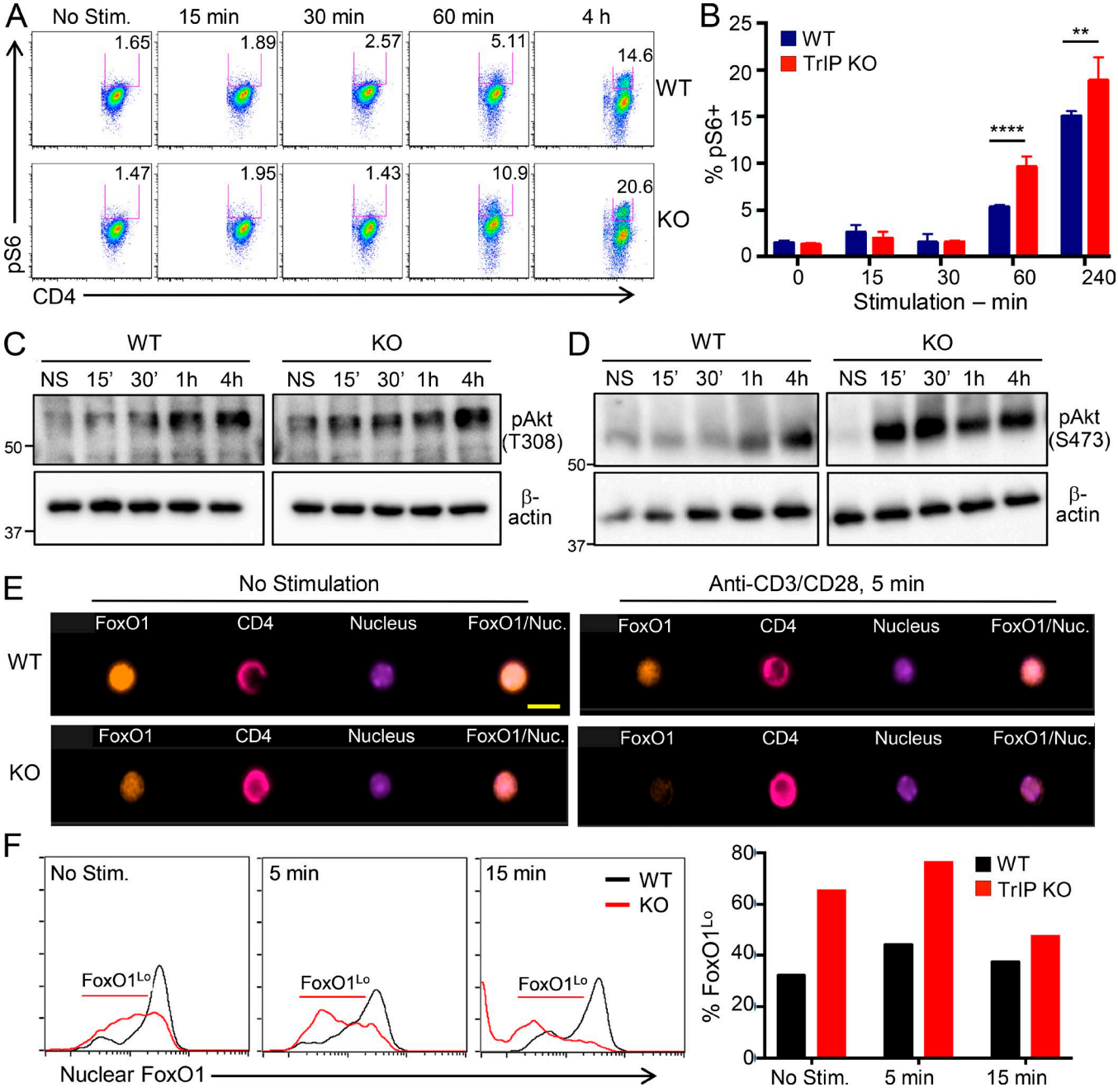

Figure 6. **Enhanced pAkt and pS6 activation in TrIP-deficient T cells.** Splenocytes and lymphocytes were isolated from WT and KO mice and stimulated with anti-CD3/CD28 for the indicated times. **(A)** Flow cytometric analysis of pS6 expression on stimulated CD4+ T cells. **(B)** Quantitation of data shown in A. **(C and D)** T cells were purified from spleen and lymph nodes of WT or TrIP KO mice and stimulated with anti-CD3/CD28 antibodies for the indicated times. Lysates were analyzed by Western blot for phospho-Akt (T308-left; S473-right) and β-actin as a loading control. Data in A–D are representative of three experiments each. **(E and F)** WT and TrIP KO CD4+ T cells were analyzed for nuclear FoxO1 staining by imaging cytometry. **(E)** Representative images showing FoxO1, CD4, and nuclear (DAPI) staining of resting and stimulated T cells. The yellow scale bar represents 10 µm. **(F)** Left: Histograms displaying the magnitude of nuclear FoxO1 in WT versus TrIP KO T cells, before and after anti-CD3/CD28 stimulation. Right: Graphical representation of the percentage of cells falling in the nuclear FoxO1Lo gate from the left histograms. Data in F represent ∼1,000 CD4+ T cells per condition, from a single experiment, representative of two that were performed. P values were calculated using two-way ANOVA with Sidak's multiple comparisons test. P values are represented with the following symbols: **, P = 0.001–0.01; and ****, P < 0.0001. Data shown represent the mean ± SEM.

proliferation and pathogen clearance. Thus, naive T cells from TrIP$^{fl/fl}$ × CD4-Cre mice were purified from spleen and lymph node and stimulated with anti-CD3 ± anti-CD28. One of the earliest cell-surface changes after T cell activation is up-regulation of CD69, a sensitive marker of TCR signaling that plays a role in delaying trafficking of nascently activated T cells out of the lymph node (Shiow et al., 2006). Thus, we noted that TrIP-deficient T cells up-regulated CD69 more robustly than did WT T cells (Fig. 9 A). A somewhat later event is the up-regulation of CD25, which is a component of the high-affinity IL-2 receptor.

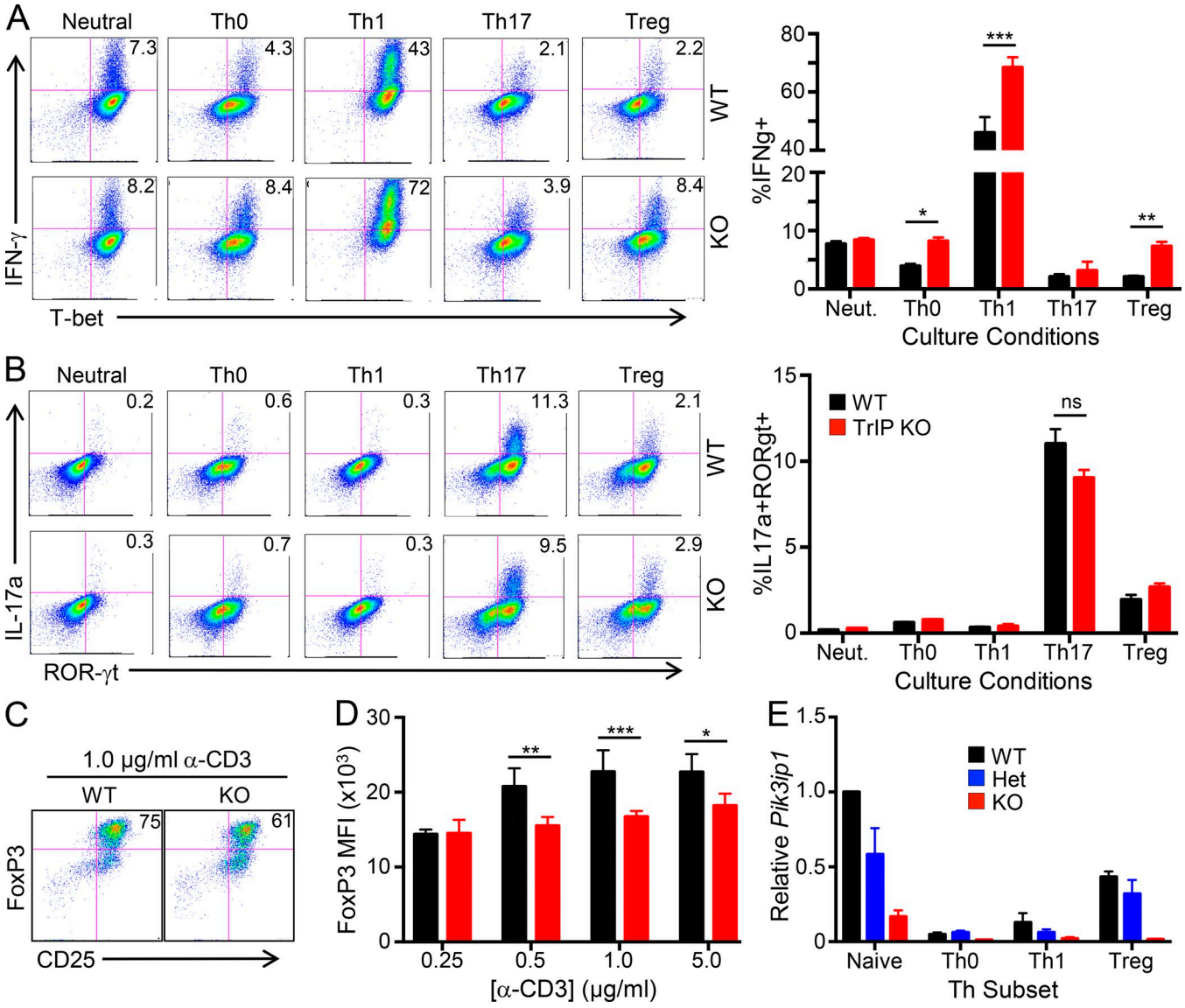

Figure 7. **TrIP KO T cells display a higher tendency for Th1 differentiation. (A–D)** Naive T cells from WT and KO mice were cultured under neutral, Th0, Th1, Th17, and iTreg conditions for 3 d, restimulated, and analyzed for IFN-γ and T-bet expression (A), IL-17a and RORγt expression (B), and Foxp3 and CD25 expression (C and D). **(E)** Naive CD4⁺ T cells from the indicated mice were stimulated under the indicated conditions, and RNA was extracted and analyzed by quantitative PCR for *Pik3ip1* message. Het, *Pik3ip1* heterozygous. Data shown are normalized to naive WT T cells. P values were calculated using two-way ANOVA with Sidak's multiple comparisons test. P values are represented with the following symbols: *, P = 0.01–0.05; **, P = 0.001–0.01; and ***, P < 0.001. Data in each panel are representative of at least three experiments. Data shown represent the mean ± SEM.

We noted higher expression of CD25 in TrIP-deficient T cells at both days 3 and 5 after stimulation (Fig. 9 B), specifically on cells stimulated with anti-CD3 alone, which is intriguing because CD25 is a known target of CD28 costimulation (Cerdan et al., 1992). Importantly, basal expression of both CD69 and CD25 was identical in naive TrIP KO versus WT T cells (Fig. S3 D). We did note a slight, but reproducible, decrease in basal levels of CD62L on naive CD8⁺ T cells lacking TrIP, which was eventually normalized over the course of initial T cell activation (Fig. S3 F). We also collected supernatants from stimulated T cells and measured secretion of IL-2 by ELISA. Thus, we observed significantly more IL-2 production from TrIP-deficient T cells, compared with WT cells, with or without CD28 costimulation (Fig. 9 C).

The PI3K pathway plays a major role in triggering T cell response to antigen via a number of processes, including proliferation. The effects on early activation discussed above, especially the increases in CD25 and IL-2, suggested that TrIP loss might also impact T cell proliferation. Naive T cells were isolated from WT and KO mice, stained with cell trace violet, and cultured on anti-CD3–coated plates in the presence or absence of anti-CD28. Cells were analyzed for proliferation at days 3 and 5 after stimulation. We found that at both time points, KO T cells had proliferated to a greater extent than WT T cells, after stimulation with either anti-CD3 alone or anti-CD3/CD28 (Fig. 9, D and E). These findings further support the model that TrIP restricts T cell activation.

To explore the role of TrIP function in vivo, we infected mice with *L. monocytogenes*, a disease model that requires effective

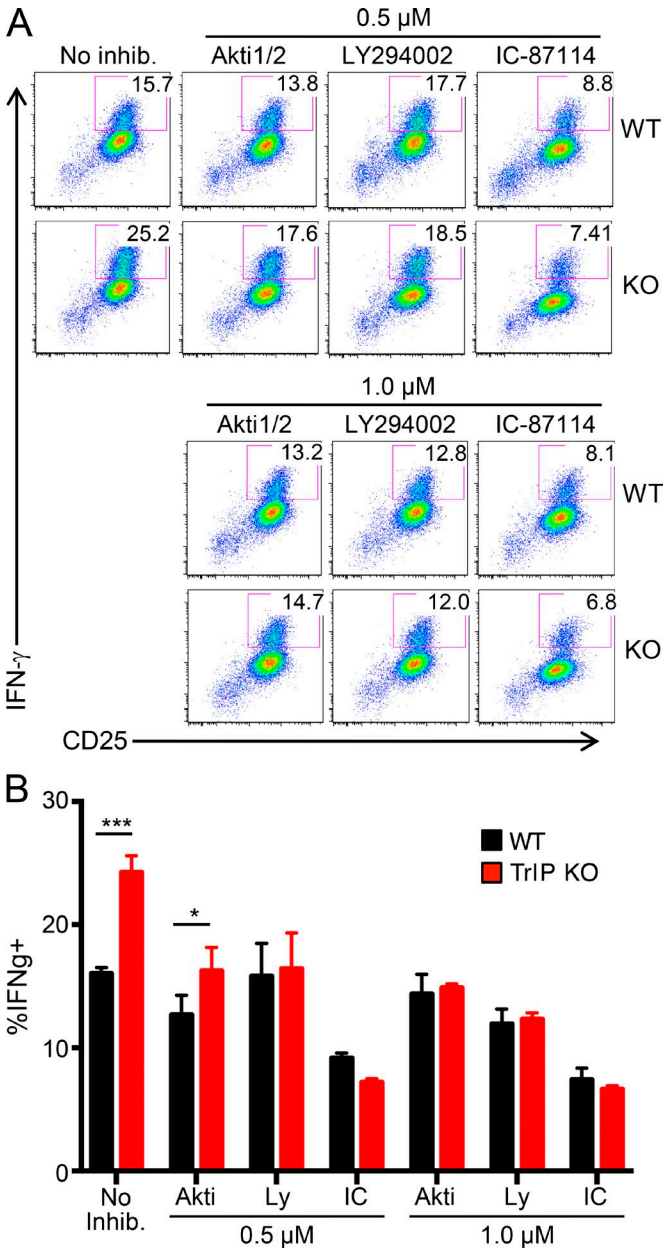

Figure 8. **Enhanced activation of TrIP-deficient T cells is reversed by PI3K/Akt pathway inhibitors. (A)** Naive T cells from WT and KO mice were cultured under Th1 conditions for 3 d in the presence of PI3K inhibitors (Akti, LY294002, and IC-87114), restimulated with PMA/ionomycin and analyzed for IFN-γ and CD25 expression. **(B)** Quantitation of A. P values (comparing WT to KO) were calculated using two-way ANOVA with Sidak's multiple comparisons test. P values are represented with the following symbols: *, P = 0.01–0.05; and ***, P < 0.001. Data in each panel are representative of at least three experiments. Data shown represent the mean ± SEM.

CD8⁺ and Th1 T cell responses for clearance of pathogen and generation of immune memory (Lara-Tejero and Pamer, 2004; Pamer, 2004). We infected mice with a relatively high dose (15,000 CFU) of *L. monocytogenes*, as we hypothesized that TrIP KO mice would be able to clear the infection more efficiently, based on the in vitro data detailed above. We observed significantly lower bacterial load from the livers of TrIP KO mice, compared with WT mice, at day 4 after infection (Fig. 9 F). Thus, the enhanced sensitivity of TrIP KO T cells described above does indeed translate to more robust in vivo activity of these cells in response to an intracellular bacterial infection.

Discussion

TrIP is a transmembrane protein that contains two identifiable domains: an extracellular kringle domain, implicated in ligand interaction in related proteins (Patthy et al., 1984; Menhart et al., 1995; Ji et al., 1998), and an intracellular p85-like domain. An initial study showed that PI3K was inhibited by TrIP through its interaction with the catalytic subunit of PI3K via the p85-like domain (Zhu et al., 2007). We also showed previously that silencing TrIP in T cells leads to up-regulation of T cell signaling (DeFrances et al., 2012). Here we sought to obtain a more complete understanding of TrIP structure and function in an immune context. Our results showed that overexpression of WT TrIP in D10 cells resulted in impaired phosphorylation of ribosomal S6 protein, as well as impaired nuclear exclusion of FoxO1 (a direct Akt target), further validating the model that TrIP inhibits the PI3K/Akt pathway. It should be noted that there has been some controversy regarding the relevance of the PI3K/Akt module in regulation of mTOR activity in T cells. Thus, while studies in many different cell types have validated the existence of such a pathway (Chi, 2012), work from Cantrell and colleagues has called into question its relevance in CD8⁺ effector T cells (Macintyre et al., 2011). Most of the experiments presented here were performed either with a CD4⁺ T cell clone or with naive murine T cells, so it may be that this pathway is wired differently in different T cell subsets (e.g., CD4⁺ versus CD8⁺), and/or in naive versus effector T cells.

In our studies, the inhibitory activity of TrIP was inversely correlated with surface expression of the protein, as we observed significant up-regulation of pS6 only when TrIP expression had been mostly down-regulated, suggesting that this down-regulation is required for efficient signaling immediately following TCR activation. Although the mechanisms behind this down-regulation have not been fully elucidated here, we present evidence that ADAM family metalloproteases are required for the loss of cell-surface TrIP after T cell activation. There is also precedent for acute down-regulation of other immune checkpoint molecules. For example, Lag3 and Tim-3 can be inducibly cleaved from the cell surface by metalloproteases, resulting in enhanced T cell activation (Li et al., 2007; Clayton et al., 2015), whereas PTEN, an intracellular inhibitor of the PI3K pathway, is down-regulated by multiple mechanisms, including post-translational modification and degradation (Hawse et al., 2015). Thus, while we have implicated ADAM family proteases in TrIP down-regulation, we cannot rule out roles for additional mechanisms.

It has been reported that kringle domains in other proteins can serve regulatory functions, including acting as sites for protein–protein interactions (Théry and Stern, 1996; Castellino and McCance, 1997; Cao et al., 2002; Tolbert et al., 2010). We therefore hypothesized that the kringle domain might serve to modulate the activity of TrIP. Indeed, the kringle domain appears to be essential for TrIP inhibitory function. A TrIP construct in which the kringle domain was deleted led to higher induction of pS6 than was observed in T cells transfected with WT TrIP or even cells

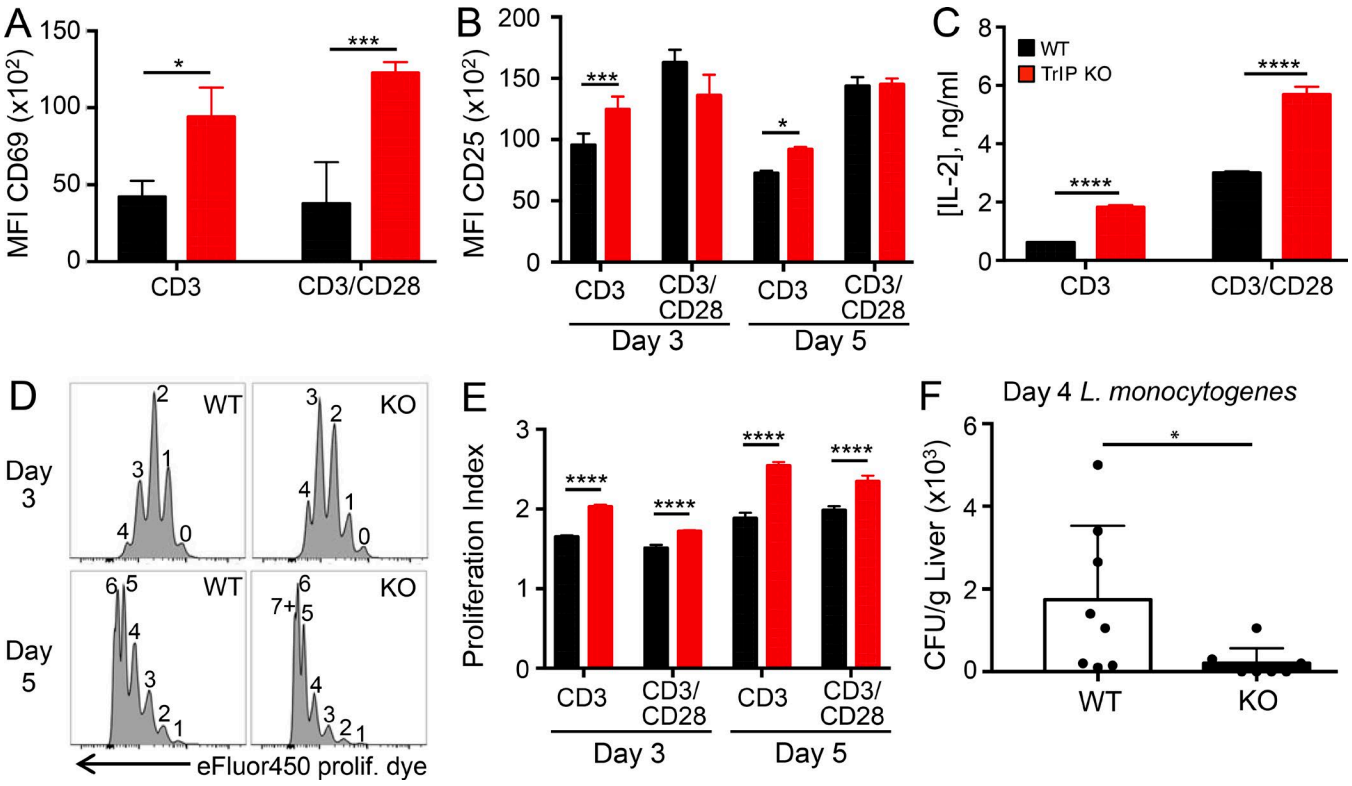

Figure 9. **TrIP KO T cells display increased proliferation and IL-2 production, and T cell–specific TrIP KO mice are less susceptible to *L. monocytogenes* infection. (A and B)** WT or TrIP naive T cells were stimulated as indicated for 24 h (A) or 3–5 d (B), then analyzed by flow cytometry for expression of CD69 (A) or CD25 (B). **(C)** WT or TrIP KO T cells were stimulated for 3 d, and supernatants were analyzed by ELISA for IL-2. **(D and E)** WT or TrIP KO CD8⁺ T cells were labeled with eFluor450 cell proliferation dye and stimulated with anti-CD3 ± anti-CD28 mAb for the indicated times. Representative flow cytometry histograms for anti-CD3 stimulation are shown in D. Compiled data from triplicate wells are shown in E. **(F)** Liver extracts from WT (CD4-Cre only) and TrIP KO mice infected with *L. monocytogenes* were obtained 4 d after infection and plated to measure bacterial burden. P values in A–C and E (WT versus KO) were calculated using two-way ANOVA with Sidak's multiple comparisons test; in F, two-tailed unpaired *t* test was used. P values are represented with the following symbols: *, P = 0.01–0.05; ***, P = 0.0001–0.001; and ****, P < 0.0001. Data shown represent the mean ± SEM.

transfected with empty vector, suggesting that this construct may function as a "dominant negative" to inhibit endogenous TrIP. Furthermore, substitution of the kringle domain with the extracellular region of hCD8, and subsequent cross-linking by α-CD8, led to diminished induction of pS6 after TCR stimulation. We show that cell-surface TrIP expression is down-regulated during the course of TCR stimulation, even in the absence of APCs, and only occurs with WT TrIP and not truncated variants, leading us to conclude that one or more ligands that activate TrIP inhibitory activity are present on T cells. How binding of a ligand, expressed by either an APC or the T cell itself, might regulate TrIP function is not clear at this point. One possibility is that the kringle domain is required for recruitment of TrIP into proximity of the TCR and/or CD28 during synapse formation. Another nonexclusive possibility is that ligand binding may cause a conformational change in TrIP that promotes the binding, and inactivation, of PI3K. Finally, a possible mechanism for which we did obtain evidence is that TrIP may undergo homotypic oligomerization, which itself could alter TrIP localization and/or activity.

The initial description of TrIP revealed a sequence in the cytoplasmic tail that bears homology to the inter-SH2 domain of the PI3K adaptor protein p85, which regulates activation of catalytic p110 subunits (Zhu et al., 2007). Confirming and extending the findings of Zhu et al. (2007), we show here that TrIP can coimmunoprecipitate the p110δ protein, which is the dominant isoform of PI3K-regulating T cell activation (Okkenhaug, 2013). Our operative model is that binding of TrIP interferes with the allosteric activation of p110 by p85. Although we cannot rule out the possibility that TrIP might regulate p110 stability, the kinetics with which PI3K activation recovers after TrIP down-regulation suggest that this is not the dominant mechanism. A third possible mechanism underlying TrIP function is through effects on the subcellular localization of p110, which could impact the accessibility of p110 to either upstream activators or substrates. Although the precise mechanism by which PI3K is activated in the immune synapse have been controversial (Okkenhaug and Fruman, 2010), such a mechanism for TrIP function could result in decreased recruitment of PI3K to CD28 and/or the TCR/CD3 complex (see model in Fig. S4). It should be noted that while this manuscript was under review, Campbell and colleagues reported a role in T cells for the protein BCAP, a positive regulator of PI3K that was previously thought to function mainly in B cells (Singh et al., 2018). In future experiments, it will be of interest to determine whether there is any functional relationship between BCAP and TrIP.

To probe the function of TrIP in primary T cells, we generated an inducible knockout model which we crossed to CD4-Cre transgenic mice, to delete TrIP in all α/β T cells. Thus, T cells from these animals were hypersensitive to stimulation through the

TCR, as shown by enhanced induction of early activation markers like CD69 expression and later events like proliferation. In addition, experiments with TrIP KO T cells validated our finding that pS6 is a relevant downstream target for monitoring TrIP activity. When we differentiated naive CD4+ T cells from TrIP KO mice, we also noted increased production of IFN-γ by Th1 cells. While we saw no obvious developmental defects or spontaneous inflammation in mice with T cell–specific TrIP deficiency, we cannot rule out the possibility that TrIP may play a subtler role in TCR repertoire selection or T cell homeostasis.

Previous work by others has shown that *L. monocytogenes* replicates for 3 d after infection of mice (Wong and Pamer, 2003). Here we observed that by day 4, TrIP knockout mice had cleared the infection, compared with WT mice that still had significant bacterial burden. Based on the typical immune response to *L. monocytogenes* infection (Wong and Pamer, 2003; Pamer, 2004), clearance of bacteria correlates with the peak of the immune response. Taken together, our results suggest that with the increased T cell signaling in the absence of TrIP, CD8 T cells from KO mice were acutely activated, leading to more rapid expansion of responding cells. Thus, due to this faster rate of expansion of effector cells, KO mice cleared bacteria faster.

Overall, our results reveal TrIP to be a potential target for modulating immune responses under conditions of infection, cancer, or autoimmunity. In the former settings, reducing the TrIP inhibitory pathway could promote more effective clearance of pathogens or tumors. Conversely, increasing TrIP activity or expression may be an effective strategy for combating pathological immune responses such as autoimmune diseases.

Materials and methods

Cell lines, transfections, and activation

The D10 Th2 T cell clone (D10.G4.1; ATCC TIB-224) was maintained in RPMI media supplemented with 10% bovine growth serum (BGS; Hyclone), penicillin, streptomycin, glutamine, and 25 U/ml recombinant human IL-2. Human embryonic kidney (HEK) 293 cells were maintained in DMEM supplemented with 10% BGS, penicillin, streptomycin, and glutamine. CH27 mouse lymphoma cells (RRID:CVCL7178) were maintained in RPMI media supplemented with 10% BGS, penicillin, streptomycin, and glutamine. For structure–function assays, using a Bio-Rad GenePulser Xcell, D10 cells were individually electroporated with control plasmid, flag-tagged WT TrIP, or Flag-tagged mutant TrIP constructs, along with pMaxGFP plasmid (encoding GFP from copepod *Pontellina plumata*). 1 d after transfection, cells were evaluated by flow cytometry for GFP expression and TrIP expression (by anti-Flag staining) using anti-DYKDDDDK APC clone L5 (BioLegend; 637308).

Transfected D10 cells were stimulated in RPMI with 3 µg/ml biotinylated anti-CD3 and anti-CD28 in the presence of 15 µg/ml streptavidin (anti-mCD3ε biotin, clone 145-2C11; Tonbo Biosciences, 30-0031-U500; anti-mCD28 biotin, clone 37.51; BD Biosciences, 553296; streptavidin; Millipore Sigma, 189730). Cells were activated for 15, 30, or 60 min. Activation was stopped with 1 ml cold PBS, followed by centrifugation and aspiration of media. For ADAM10/17 inhibition studies, 1 µM of a dual ADAM 10 and ADAM 17 inhibitor GW280264X (AOBIOUS; AOB3632) was incubated with cells for 30 min before stimulation.

For p110δ interaction assays, flag-tagged TrIP variants and HA-tagged p110δ were transfected into HEK293 cells using TransIT-LT1 (Mirus) according to the manufacturer's protocol. Cells were evaluated by Western blot for expression using Roche anti-HA (clone 12CA5; 11-583-816-001) and BioLegend Direct-Blot HRP anti-DYKDDDDK (clone L5; 637311).

T cell/APC cocultures

CH27 cells were pulsed with 100 µg/ml chicken conalbumin (Sigma; C7786) 1 d before mixing with D10 cells. D10 cells were mixed in a 1:1 ratio with either pulsed unpulsed CH27 cells for 15, 30, and 60 min. Reactions were quenched by placing cells on ice, adding 1 ml PBS, and centrifugating to settle cells and decant activation media. Cells were then stained with anti-DYKDDDDK APC clone L5 (BioLegend; 637308), anti-mouse CD19 violet Fluor 450 (clone 1D3; Tonbo Biosciences, 75-0193-U025), and anti-mouse CD4 Brilliant Violet 510 (clone GK1.5; BioLegend, 100449). Cells were washed three times in PBS, fixed and permeabilized with eBioscience Foxp3/transcription factor staining buffer (00-5523-00), and then stained with anti-pS6 (S235/236) Alexa Fluor 647 (clone D57.2.2E; Cell Signaling, 5316S).

Mice

Mice with a floxed *Pik3ip1* gene (Pik3ip1$^{fl/fl}$) were generated by inGenious Targeting Laboratory using C57BL/6 ES cells. CD4-Cre mice on a C57BL/6 background were originally purchased from Taconic (previously backcrossed for more than nine generations to C57BL/6), then maintained by breeding to C57BL/6J mice (The Jackson Laboratory), and were used as WT controls. All control animals were either littermates of KO mice or derived from in-house breeding in the same facility and room. Mice were age-matched within experiments, with approximately equal numbers of male and female animals. Animals were maintained in facilities of the University of Pittsburgh Division of Laboratory Animal Resources. All animal studies were performed in accordance with University of Pittsburgh Institutional Animal Care and Use Committee procedures.

T cell purification and differentiation

Total or CD4+ α/β T cells from spleens and lymph nodes of naive mice were purified by magnetic separation using T cell isolation kits from Miltenyi Biotec. The purity of the final cell population was >90%. T cells were activated with plate-bound anti-CD3 (clone 145-2C11; Bio X Cell InVivoMab, BE0001-1), along with soluble anti-CD28 (clone 37.51; eBioscience, 14-0281-85), in complete medium (RPMI medium supplemented with 10% BGS, 2 mM L-glutamine, 100 U/ml penicillin, 100 µg/ml streptomycin, 50 µM 2-mercaptoethanol, Hepes, and sodium pyruvate). For Th1 differentiation, cells were cultured in the presence of recombinant murine IL-12 (10 ng/ml), anti–IL-4 (10 µg/ml), and recombinant human IL-2 (50 U/ml). For Th17 differentiation, cells were cultured in the presence of recombinant hTGF-β (2.5 ng/ml), recombinant mIL-6 (20 ng/ml), plus anti–IFN-γ (10 µg/ml), anti–IL-4 (10 µg/ml), and anti–IL-2 (20 µg/ml) neutralizing antibodies. For iTreg differentiation, cells were cultured in the

presence of anti–IL-4 and anti–IFN-γ neutralizing antibodies (10 µg each) plus recombinant hTGFβ2 (10 ng/ml) and recombinant hIL-2 (50 U/ml), with varying concentrations of anti-CD3 (0.25, 0.5, 1.0, and 5.0 µg/ml) and 1 µg/ml anti-CD28. Cells were cultured for 3 d under Th differentiation conditions and then stimulated for 4 h with PMA (50 ng/ml) and ionomycin (1.33 µM) in the presence of Golgi Plug (BD Biosciences; 51-2301KZ). Cells were then harvested and analyzed by flow cytometry.

Th cell differentiation reagents were as follows: murine IL-12 (Miltenyi Biotec; 130-096-707); murine IL-6 (Miltenyi Biotec; 130-094-065); recombinant hTGF-β (Sigma; SRP3170-5UG); anti-mouse IL-4 clone 11B11 (Bio X Cell; BE0045); anti–mIL-2 clone S4B6-1 (Bio X Cell; BE0043); and anti–mIFN-γ clone XMG1.2 (Bio X Cell; BE0055).

The following antibodies and dyes were used for flow cytometry: anti-mCD4 Brilliant Violet 510 clone GK1.5 (BioLegend; 100449); Ghost Dye Red 780 (Tonbo Biosciences; 13-0865-T100); V450-anti-mFoxp3 clone MF23 (BD Horizon; 561293); anti-mouse RORγt-PE (clone Q31-378; BD Biosciences, 562607); anti-mouse IL-17A PerCP-Cy5.5 (clone eBio17B7; eBioscience, 45-7177-80); anti-mFoxp3 APC (clone FJK-16s; eBioscience, 17-5773-82); anti-mTbet eFluor 660 (clone eBio4B10; eBioscience, 50-5825-82); anti–mIFN-γ PE-Cy7 (clone XMG1.2; Tonbo Biosciences, 60-7311-U025); and anti-mouse CD25 FITC (clone PC61.5; Tonbo Biosciences, 35-0251-U100).

T cell activation

Splenocytes and lymphocytes obtained from WT and conditional TrIP KO mice were stimulated in complete RPMI with 3 µg/ml biotinylated anti-CD3 and anti-CD28 in the presence of 15 µg/ml streptavidin (anti-mCD3ε biotin, clone 145-2C11; Tonbo Biosciences, 30-0031-U500; anti-mCD28 biotin, clone 37.51; BD Biosciences, 553296; streptavidin; Millipore Sigma, 189730). Cells were activated for 15, 30, or 60 min or 4 h. Activation was stopped with 1 ml cold PBS, followed by centrifugation, aspiration of media, and lysis or fixation.

The following antibodies and dyes were used for flow cytometry: anti-mCD4 Brilliant Violet 510 (clone GK1.5; BioLegend, 100449); anti-mCD8α v450 (clone 53-6.7; Tonbo Biosciences, 75-0081-U100); anti-pS6 (S235/236) Alexa Fluor 647 (clone D57.2.2E; Cell Signaling, 5316S); anti-mCD69 FITC (clone H1.2F3; BD Biosciences, 557392); and Ghost Dye Red 780 (Tonbo Biosciences; 13-0865-T100).

T cell proliferation

CD4 T cells from spleens of naive mice were purified by magnetic separation using the Miltenyi Biotec naive CD4 T cell isolation kit (130-104-453). The purity of the final cell population was >90%. Before activation, T cells were labeled with cell proliferation dye eFluor 450 (eBioscience; 65-0842) following the manufacturer's protocol. T cells were then activated with plate-bound anti-CD3 (clone 145-2C11; Bio X Cell InVivoMab BE0001-1) in complete RPMI medium (supplemented with 10% BGS, 2 mM L-glutamine, 100 U/ml penicillin, 100 µg/ml streptomycin, 50 µM 2-mercaptoethanol, Hepes, and sodium pyruvate) in the presence or absence of 1 µg/ml anti-CD28 (clone 37.51; eBioscience, 14-0281-85). Cells were then cultured for 3 or 5 d before harvesting and analysis by flow cytometry.

Quantitative PCR

RNA was extracted using the Qiagen RNeasy Mini Kit (74106) and reverse-transcribed to generate cDNA with the Applied Biosystems High Capacity cDNA Reverse Transcription Kit (4368813). Quantitative real-time PCR assays were performed with Power SYBR Green PCR Master Mix (Applied Biosystems; 4367659) on a Step-One Plus Real Time PCR system. The abundance of TrIP mRNA was normalized to that of mGAPDH as calculated with the $2^{-\Delta\Delta CT}$ method. The following primers were used: forward, 5′-ATGCTGTTGGCTTTGGGTACAC-3′; and reverse, 5′-CGGCAG TAGTTGTGGTTGC-3′.

Flow cytometry

Before staining, cells were washed in staining buffer (1% BGS-supplemented PBS). For extracellular staining, cells were stained at 4°C with antibodies resuspended in staining buffer. For intracellular staining, cells were washed three times to remove excess extracellular staining and then fixed and permeabilized with either the eBioscience Foxp3/Transcription factor staining buffer set (00-5523-00) or the BD Biosciences cytofix/perm kit (554714) for transcription factor and cytosol analysis, respectively. Fixed and permeabilized cells were then stained at 4°C with antibodies resuspended in permeabilization buffer from the respective kits.

Imaging flow cytometry

For FoxO1 assays, D10 cells were individually electroporated (as described in Cell lines, transfections, and activation) with control plasmid or flag-tagged WT TrIP constructs, along with pMaxGFP plasmid (encoding GFP from copepod *P. plumata*). 1 d after transfection, cells were evaluated by flow cytometry for GFP expression and TrIP expression (by anti-Flag staining) using anti-DYK DDDDK APC clone L5 (BioLegend; 637308). Transfected D10 cells were then sorted for GFP-positive cells on a BD FACS ARIA IIu using the 70-µm nozzle at 70 psi. GFP was excited by the 488-nm laser and read using a 530/30 filter. Sorted D10 cells were stimulated as described in Cell lines, transfections, and activation. Activation was stopped with 1 ml cold PBS, followed by centrifugation and aspiration of media. Sorted D10 cells were then fixed and intracellularly stained as described below for splenocytes. Splenocytes from WT and conditional TrIP KO mice were stimulated as described in T cell activation for the listed time points. Activation was stopped with 1 ml cold PBS, followed by centrifugation, aspiration of media, staining, and fixation.

For extracellular staining, cells were stained with staining buffer (1% BGS-supplemented PBS) using anti-mCD4 PE-Cyanine7 (clone GK 1.5; Tonbo Biosciences, 60-0041-U100). For intracellular staining, cells were washed three times to remove excess extracellular staining and then fixed and permeabilized with the eBioscience Foxp3/Transcription factor staining buffer set (00-5523-00). Fixed and permeabilized cells were then stained at 4°C with antibodies resuspended in permeabilization buffer from the same eBioscience Foxp3/Transcription factor staining kit. The following intracellular stains were used: FoxO1 (C29H4) rabbit mAb (Cell Signaling; 2880S) with Alexa Fluor 594 donkey anti-rabbit IgG (clone Poly4064; 406418) as a secondary stain. DAPI dilactate (Molecular Probes; D3571) was used for DNA/nuclear staining.

Imaging cytometry data on fixed and stained cells were acquired on an Amnis ImageStreamX Mark II running INSPIRE software (Millipore). Analysis was performed using IDEAS software (Millipore). First, focused cells, based on the gradient root mean square feature, were identified. Singlets were identified by the aspect ratio and area of bright-field data. In analyzing primary T cell data, we gated on CD4 T cells via the intensity of that channel. A nucleus intensity mask was made from DAPI staining. This mask was used to determine FoxO1 intensity in the nucleus. A gate of low FoxO1 nuclear signal was then set based on the unstimulated control samples. Approximately 1,000 cells are represented in the summary histograms and bar graphs of primary cells, and 3,000–4,000 cells are represented in the D10 T cell data. The typical spread of the data is illustrated by the histograms in Fig. 6 F.

Western blotting analysis and immunoprecipitations

Cells were lysed in ice-cold NP-40 lysis buffer (1% NP-40, 1 mM EDTA, 20 mM Tris-HCl, pH 7.4, and 150 mM NaCl) for both protein analysis and immunoprecipitation. Immunoprecipitation was performed by mixing lysate with 20 µl M2 anti-Flag agarose beads for 3 h at 4°C. Proteins were eluted from beads by mixing Lysate with 1× SDS (containing 5% β-mercaptoethanol) and boiling at 95°C for 10 min. For Western blot analysis, proteins were resolved by 10% SDS-PAGE and transferred onto polyvinylidene difluoride membranes, which were then blocked in 4% BSA. The membranes were then incubated with the primary antibodies overnight. This was followed by incubating the membrane with HRP-conjugated secondary antibodies for 2 h before detection with the SuperSignal West Pico ECL substrate (Thermo Fisher Scientific) and imaging on a Protein Simple FluorChem M.

Western blot and CoIP reagents

Reagents used were anti-HA (12CA5; Roche, 11-583-816-001); anti-Flag M2 Affinity Gel (Sigma; A2220); and direct-Blot HRP anti-DYKDDDDK (clone L5; BioLegend, 637311).

L. monocytogenes infection

Control WT (CD4-Cre alone) and Pik3ip1$^{fl/fl}$ × CD4-Cre mice were infected intravenously with 15,000 CFU *L. monocytogenes* in 200 µl PBS. Bacterial titers were quantified by lysing whole livers in PBS, plating a 1:10 dilution on brain-heart infusion agar plates, and culturing overnight. Cells were stained with the following antibodies and dyes and analyzed by flow cytometry: Ghost Red 780 viability dye (Tonbo Biosciences; 13-0865-T100); anti-mCD4 Brilliant Violet 510 (clone GK1.5; BioLegend, 100449); anti-mCD8a PE (clone 53-6.7; Tonbo Biosciences, 50-0081-U100); anti-mCD62L PerCP-Cy5.5 (clone MEL-14; eBioscience, 45-0621-80); anti-mKLRG1 FITC (clone 2F1; Tonbo Biosciences, 35-5893-U100); anti-mCD127 PE-Cy7 (clone A7R34; Tonbo Biosciences, 60-1271-U025); and anti-mCD44 violet Fluor 450 (clone IM7; Tonbo Biosciences, 75-0441-U025). All Ab staining was performed at 4°C in PBS containing 1% BGS and 0.1% sodium azide. GP33 tetramers were provided as APC fluorophore-conjugated tetramers by the NIH tetramer core facility and used for identification of gp33-specific CD8$^+$ and CD4$^+$ T cells.

Online supplemental material

Fig. S1 shows the effects of PI3K inhibition on pS6 induction in the D10 T cell line and primary T cells, as well as the effect of ectopic TrIP expression on FoxO1 nuclear localization. Fig. S2 shows control experiments and alternative analysis of in vitro experiments referred to in Figs. 1, 2, 3, 4, and 5. Fig. S3 shows data on T cell development and the baseline phenotype of T cells in mice with T cell–specific TrIP KO. Fig. S4 presents a model for the function of TrIP in proximal TCR/CD3 and CD28 signaling.

Acknowledgments

We thank Sue Kaech (Salk Institute), for providing LM stock and Marie DeFrances (Department of Pathology, University of Pittsburgh) and members of the Kane laboratory for helpful discussions and feedback on the manuscript.

This work was supported by Public Health Service (PHS) grants AI126845 and AI095730 and by a supplement to PHS grant AI103022 (to L.P. Kane), and by startup funds from the University of Pittsburgh (to L.M. D'Cruz). This work also benefitted from an ImageStreamX MarkII, funded by PHS grant S10OD011925.

S. Kataoka is an employee of Asahi Kasei Corporation. The other authors declare no competing financial interests.

U.U. Uche designed and performed most experiments and wrote the manuscript. A.R. Piccirillo performed *Listeria* infections. S. Kataoka and S.J. Grebinoski performed experiments. L.M. D'Cruz designed and analyzed *Listeria* infection experiments and edited the manuscript. L.P. Kane obtained funding for the study, designed and analyzed experiments, and cowrote the manuscript.

Submitted: 7 November 2017
Revised: 27 June 2018
Accepted: 19 October 2018

References

Agoulnik, I.U., M.C. Hodgson, W.A. Bowden, and M.M. Ittmann. 2011. INPP4B: the new kid on the PI3K block. *Oncotarget*. 2:321–328. https://doi.org/10.18632/oncotarget.260

Antignano, F., M. Ibaraki, C. Kim, J. Ruschmann, A. Zhang, C.D. Helgason, and G. Krystal. 2010. SHIP is required for dendritic cell maturation. *J. Immunol.* 184:2805–2813. https://doi.org/10.4049/jimmunol.0903170

Cantley, L.C. 2002. The phosphoinositide 3-kinase pathway. *Science*. 296:1655–1657. https://doi.org/10.1126/science.296.5573.1655

Cao, Y., R. Cao, and N. Veitonmäki. 2002. Kringle structures and antiangiogenesis. *Curr. Med. Chem. Anticancer Agents*. 2:667–681. https://doi.org/10.2174/1568011023353705

Carracedo, A., and P.P. Pandolfi. 2008. The PTEN-PI3K pathway: of feedbacks and cross-talks. *Oncogene*. 27:5527–5541. https://doi.org/10.1038/onc.2008.247

Castellino, F.J., and S.G. McCance. 1997. The kringle domains of human plasminogen. *Ciba Found. Symp.* 212:46–60, discussion :60–65.

Cerdan, C., Y. Martin, M. Courcoul, H. Brailly, C. Mawas, F. Birg, and D. Olive. 1992. Prolonged IL-2 receptor alpha/CD25 expression after T cell activation via the adhesion molecules CD2 and CD28. Demonstration of combined transcriptional and post-transcriptional regulation. *J. Immunol.* 149:2255–2261.

Chi, H. 2012. Regulation and function of mTOR signalling in T cell fate decisions. *Nat. Rev. Immunol.* 12:325–338. https://doi.org/10.1038/nri3198

Christen, M.T., P. Frank, J. Schaller, and M. Llinás. 2010. Human plasminogen kringle 3: solution structure, functional insights, phylogenetic landscape. *Biochemistry.* 49:7131–7150. https://doi.org/10.1021/bi100687f

Clayton, K.L., M.B. Douglas-Vail, A.K. Nur-ur Rahman, K.E. Medcalf, I.Y. Xie, G.M. Chew, R. Tandon, M.C. Lanteri, P.J. Norris, S.G. Deeks, et al. 2015. Soluble T cell immunoglobulin mucin domain 3 is shed from CD8+ T cells by the sheddase ADAM10, is increased in plasma during untreated HIV infection, and correlates with HIV disease progression. *J. Virol.* 89:3723–3736. https://doi.org/10.1128/JVI.00006-15

DeFrances, M.C., D.R. Debelius, J. Cheng, and L.P. Kane. 2012. Inhibition of T-cell activation by PIK3IP1. *Eur. J. Immunol.* 42:2754–2759. https://doi.org/10.1002/eji.201141653

Dillon, L.M., and T.W. Miller. 2014. Therapeutic targeting of cancers with loss of PTEN function. *Curr. Drug Targets.* 15:65–79. https://doi.org/10.2174/1389450114666140106100909

Engelman, J.A. 2009. Targeting PI3K signalling in cancer: opportunities, challenges and limitations. *Nat. Rev. Cancer.* 9:550–562. https://doi.org/10.1038/nrc2664

Fresno Vara, J.A., E. Casado, J. de Castro, P. Cejas, C. Belda-Iniesta, and M. González-Barón. 2004. PI3K/Akt signalling pathway and cancer. *Cancer Treat. Rev.* 30:193–204. https://doi.org/10.1016/j.ctrv.2003.07.007

Fruman, D.A. 2007. The role of class I phosphoinositide 3-kinase in T-cell function and autoimmunity. *Biochem. Soc. Trans.* 35:177–180. https://doi.org/10.1042/BST0350177

Fruman, D.A., R.E. Meyers, and L.C. Cantley. 1998. Phosphoinositide kinases. *Annu. Rev. Biochem.* 67:481–507. https://doi.org/10.1146/annurev.biochem.67.1.481

Han, J.M., S.J. Patterson, and M.K. Levings. 2012. The Role of the PI3K Signaling Pathway in CD4(+) T Cell Differentiation and Function. *Front. Immunol.* 3:245. https://doi.org/10.3389/fimmu.2012.00245

Haughton, G., L.W. Arnold, G.A. Bishop, and T.J. Mercolino. 1986. The CH series of murine B cell lymphomas: neoplastic analogues of Ly-1+ normal B cells. *Immunol. Rev.* 93:35–51. https://doi.org/10.1111/j.1600-065X.1986.tb01501.x

Hawse, W.F., R.P. Sheehan, N. Miskov-Zivanov, A.V. Menk, L.P. Kane, J.R. Faeder, and P.A. Morel. 2015. Cutting Edge: Differential Regulation of PTEN by TCR, Akt, and FoxO1 Controls CD4+ T Cell Fate Decisions. *J. Immunol.* 194:4615–4619. https://doi.org/10.4049/jimmunol.1402554

He, X., Z. Zhu, C. Johnson, J. Stoops, A.E. Eaker, W. Bowen, and M.C. DeFrances. 2008. PIK3IP1, a negative regulator of PI3K, suppresses the development of hepatocellular carcinoma. *Cancer Res.* 68:5591–5598. https://doi.org/10.1158/0008-5472.CAN-08-0025

Hedrick, S.M., R. Hess Michelini, A.L. Doedens, A.W. Goldrath, and E.L. Stone. 2012. FOXO transcription factors throughout T cell biology. *Nat. Rev. Immunol.* 12:649–661. https://doi.org/10.1038/nri3278

Huynh, A., R. Zhang, and L.A. Turka. 2014. Signals and pathways controlling regulatory T cells. *Immunol. Rev.* 258:117–131. https://doi.org/10.1111/imr.12148

Irving, B.A., and A. Weiss. 1991. The cytoplasmic domain of the T cell receptor zeta chain is sufficient to couple to receptor-associated signal transduction pathways. *Cell.* 64:891–901. https://doi.org/10.1016/0092-8674(91)90314-O

Ji, W.R., F.J. Castellino, Y. Chang, M.E. Deford, H. Gray, X. Villarreal, M.E. Kondri, D.N. Marti, M. Llinás, J. Schaller, et al. 1998. Characterization of kringle domains of angiostatin as antagonists of endothelial cell migration, an important process in angiogenesis. *FASEB J.* 12:1731–1738. https://doi.org/10.1096/fasebj.12.15.1731

Kane, L.P., M.N. Mollenauer, and A. Weiss. 2004. A proline-rich motif in the C terminus of Akt contributes to its localization in the immunological synapse. *J. Immunol.* 172:5441–5449. https://doi.org/10.4049/jimmunol.172.9.5441

Lara-Tejero, M., and E.G. Pamer. 2004. T cell responses to Listeria monocytogenes. *Curr. Opin. Microbiol.* 7:45–50. https://doi.org/10.1016/j.mib.2003.12.002

Li, N., C.J. Workman, S.M. Martin, and D.A. Vignali. 2004. Biochemical analysis of the regulatory T cell protein lymphocyte activation gene-3 (LAG-3; CD223). *J. Immunol.* 173:6806–6812. https://doi.org/10.4049/jimmunol.173.11.6806

Li, N., Y. Wang, K. Forbes, K.M. Vignali, B.S. Heale, P. Saftig, D. Hartmann, R.A. Black, J.J. Rossi, C.P. Blobel, et al. 2007. Metalloproteases regulate T-cell proliferation and effector function via LAG-3. *EMBO J.* 26:494–504. https://doi.org/10.1038/sj.emboj.7601520

Macintyre, A.N., D. Finlay, G. Preston, L.V. Sinclair, C.M. Waugh, P. Tamas, C. Feijoo, K. Okkenhaug, and D.A. Cantrell. 2011. Protein kinase B controls transcriptional programs that direct cytotoxic T cell fate but is dispensable for T cell metabolism. *Immunity.* 34:224–236. https://doi.org/10.1016/j.immuni.2011.01.012

Menhart, N., G.J. Hoover, S.G. McCance, and F.J. Castellino. 1995. Roles of individual kringle domains in the functioning of positive and negative effectors of human plasminogen activation. *Biochemistry.* 34:1482–1488. https://doi.org/10.1021/bi00005a003

Mikels, A., Y. Minami, and R. Nusse. 2009. Ror2 receptor requires tyrosine kinase activity to mediate Wnt5A signaling. *J. Biol. Chem.* 284:30167–30176. https://doi.org/10.1074/jbc.M109.041715

Newton, R.H., and L.A. Turka. 2012. Regulation of T cell homeostasis and responses by pten. *Front. Immunol.* 3:151. https://doi.org/10.3389/fimmu.2012.00151

Okkenhaug, K. 2013. Signaling by the phosphoinositide 3-kinase family in immune cells. *Annu. Rev. Immunol.* 31:675–704. https://doi.org/10.1146/annurev-immunol-032712-095946

Okkenhaug, K., and D.A. Fruman. 2010. PI3Ks in lymphocyte signaling and development. *Curr. Top. Microbiol. Immunol.* 346:57–85.

Okkenhaug, K., and B. Vanhaesebroeck. 2003. PI3K-signalling in B- and T-cells: insights from gene-targeted mice. *Biochem. Soc. Trans.* 31:270–274. https://doi.org/10.1042/bst0310270

Pamer, E.G. 2004. Immune responses to Listeria monocytogenes. *Nat. Rev. Immunol.* 4:812–823. https://doi.org/10.1038/nri1461

Patthy, L., M. Trexler, Z. Váli, L. Bányai, and A. Váradi. 1984. Kringles: modules specialized for protein binding. Homology of the gelatin-binding region of fibronectin with the kringle structures of proteases. *FEBS Lett.* 171:131–136. https://doi.org/10.1016/0014-5793(84)80473-1

Sauer, S., L. Bruno, A. Hertweck, D. Finlay, M. Leleu, M. Spivakov, Z.A. Knight, B.S. Cobb, D. Cantrell, E. O'Connor, et al. 2008. T cell receptor signaling controls Foxp3 expression via PI3K, Akt, and mTOR. *Proc. Natl. Acad. Sci. USA.* 105:7797–7802. https://doi.org/10.1073/pnas.0800928105

Shiow, L.R., D.B. Rosen, N. Brdicková, Y. Xu, J. An, L.L. Lanier, J.G. Cyster, and M. Matloubian. 2006. CD69 acts downstream of interferon-alpha/beta to inhibit S1P1 and lymphocyte egress from lymphoid organs. *Nature.* 440:540–544. https://doi.org/10.1038/nature04606

Singh, M.D., M. Ni, J.M. Sullivan, J.A. Hamerman, and D.J. Campbell. 2018. B cell adaptor for PI3-kinase (BCAP) modulates $CD8^+$ effector and memory T cell differentiation. *J. Exp. Med.* 215:2429–2443. https://doi.org/10.1084/jem.20171820

Théry, C., and C.D. Stern. 1996. Roles of kringle domain-containing serine proteases in epithelial-mesenchymal transitions during embryonic development. *Acta Anat. (Basel).* 156:162–172. https://doi.org/10.1159/000147844

Tolbert, W.D., J. Daugherty-Holtrop, E. Gherardi, G. Vande Woude, and H.E. Xu. 2010. Structural basis for agonism and antagonism of hepatocyte growth factor. *Proc. Natl. Acad. Sci. USA.* 107:13264–13269. https://doi.org/10.1073/pnas.1005183107

Wong, P., and E.G. Pamer. 2003. Feedback regulation of pathogen-specific T cell priming. *Immunity.* 18:499–511. https://doi.org/10.1016/S1074-7613(03)00081-5

Wong, C.C., I. Martincorena, A.G. Rust, M. Rashid, C. Alifrangis, L.B. Alexandrov, J.C. Tiffen, C. Kober, A.R. Green, C.E. Massie, et al. Chronic Myeloid Disorders Working Group of the International Cancer Genome Consortium. 2014. Inactivating CUX1 mutations promote tumorigenesis. *Nat. Genet.* 46:33–38. https://doi.org/10.1038/ng.2846

Zhu, Z., X. He, C. Johnson, J. Stoops, A.E. Eaker, D.S. Stoffer, A. Bell, R. Zarnegar, and M.C. DeFrances. 2007. PI3K is negatively regulated by PIK3IP1, a novel p110 interacting protein. *Biochem. Biophys. Res. Commun.* 358:66–72. https://doi.org/10.1016/j.bbrc.2007.04.096